Inorganic Chemistry

including bioinorganic chemistry

March 4, 2013
Volume 52, Number 5
pubs.acs.org/IC

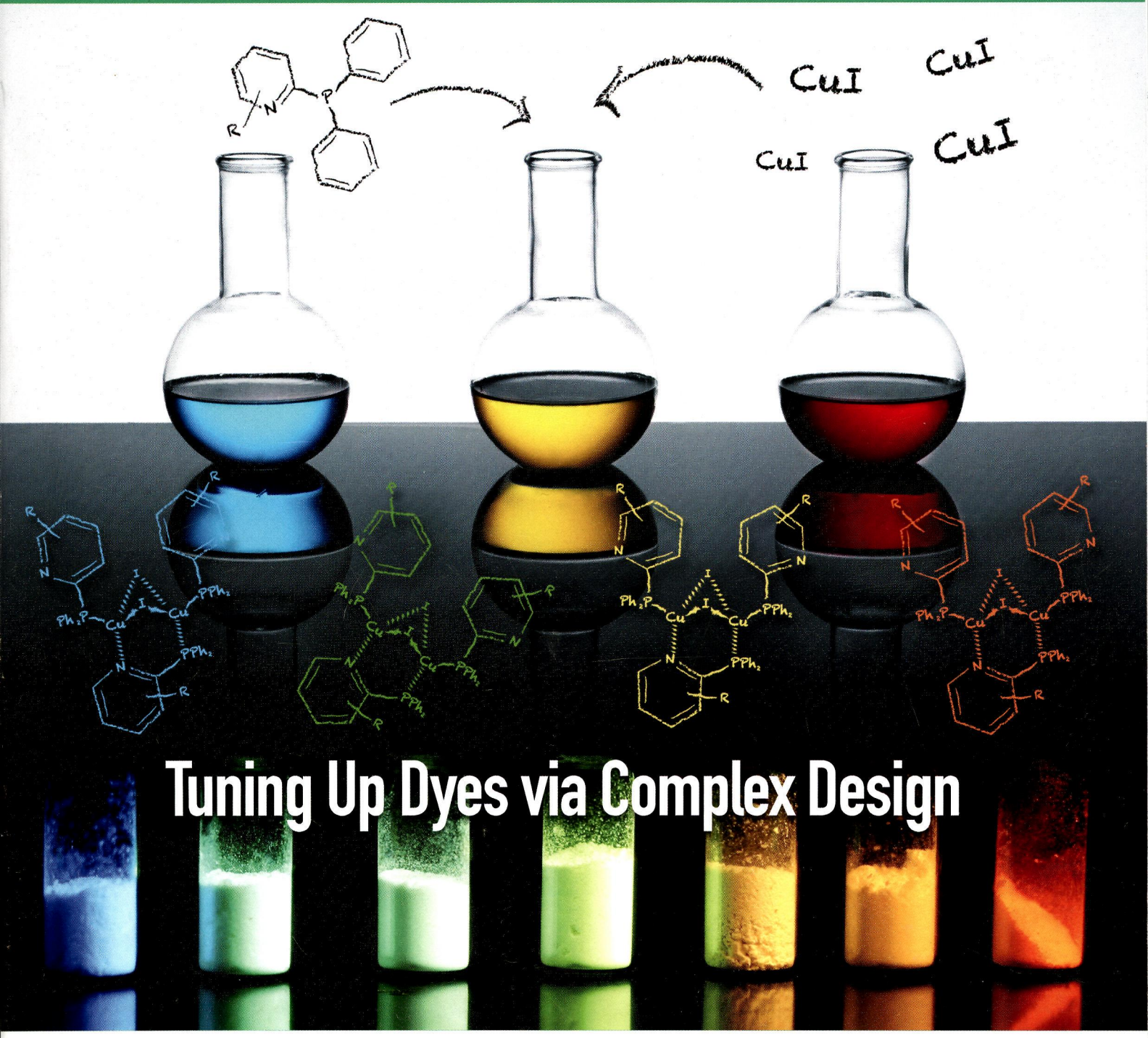

Tuning Up Dyes via Complex Design

ACS Publications
MOST TRUSTED. MOST CITED. MOST READ.

www.acs.org

Inorganic Chemistry

MARCH 4, 2013
VOLUME 52 ISSUE 5
INOCAJ 52(5) 2259–2786 (2013)
ISSN 0020-1669
Registered in the U.S. Patent and Trademark Office

ON THE COVER: A new class of highly emitting copper(I) complexes is presented using a modular approach based on a bidentate P^N ligand system. By means of electron donors or acceptors as substituents on the ligands, the LUMO of the corresponding complex is shifted in order to tune the emission wavelength across the whole visible range from blue to red. See D. M. Zink, M. Bächle, T. Baumann, M. Nieger, M. Kühn, C. Wang, W. Klopper, U. Monkowius, T. Hofbeck, H. Yersin, and S. Bräse, p 2292.

Communications

2265 S dx.doi.org/10.1021/ic302375z

Three-Dimensional Zinc(II) and Cadmium(II) Coordination Frameworks with *N,N,N′,N′*-Tetrakis(pyridin-4-yl)methanediamine: Structure, Photoluminescence, and Catalysis

Jong Won Shin, Jeong Mi Bae, Cheal Kim,* and Kil Sik Min*

Coordination polymer networks, i.e., $[Zn(tpmd)(H_2O)](NO_3)_2{\cdot}7H_2O$ (**1**) and $[Cd(tpmd)(H_2O)_2](NO_3)_2{\cdot}4H_2O{\cdot}4CH_3OH$ (**2**), were assembled from $M^{II}(NO_3)_2$ hydrates and *N,N,N′,N′*-tetrakis(pyridin-4-yl)methanediamine (tpmd) in CH_3OH and characterized. Both compounds feature three-dimensional network structures formed from coordination of the metal ions to the tpmd ligands. Also, both compounds exhibit strong emission and show very efficient catalytic activity toward the transesterification of various esters.

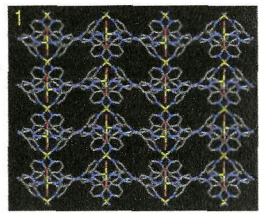

2268 S dx.doi.org/10.1021/ic302578a

Ethylene Tri- and Tetramerization: a Steric Parameter Selectivity Switch from X-ray Crystallography and Computational Analysis

Nicoline Cloete, Hendrik G. Visser,* Ilana Engelbrecht, Matthew J. Overett, William F. Gabrielli, and Andreas Roodt*

A steric parameter ($\theta_{N\text{-}sub}$) is introduced to describe the steric bulk at the nitrogen atom on a range of PNP ligands used in ethylene tri- and tetramerization. A specific tendency is observed for an increase in the bulkiness (increased value of $\theta_{N\text{-}sub}$) of the substituents on the nitrogen atom toward 1-hexene and 1-octene selectivity.

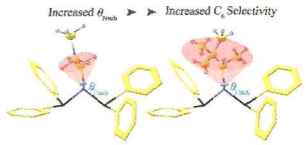

2271 S dx.doi.org/10.1021/ic302590g

Direct Synthesis of Ligand-Based Radicals by the Addition of Bipyridine to Chromium(II) Compounds

Wen Zhou, Addison N. Desnoyer, James A. Bailey, Brian O. Patrick, and Kevin M. Smith*

Chromium(III) complexes with ligand-based radicals and $S = 1$ spin states were synthesized by the reaction of 2,2′-bipyridine (bpy) with Cp_2Cr or $Cr[(OCtBu)_2CH]_2$, while the same reaction with $Cr[N(SiMe_3)_2]_2(THF)_2$ gave an $S = 2$ complex with a neutral bpy ligand.

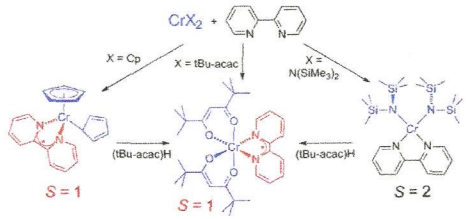

2274 S dx.doi.org/10.1021/ic302617b

Heteronuclear $Ru^{II}Ag^{I}$ Complexes Having a Pyrroloquinolinequinone Derivative as a Bridging Ligand

Hiroumi Mitome, Tomoya Ishizuka, Yoshihiko Shiota, Kazunari Yoshizawa, and Takahiko Kojima*

Herein, we report the synthesis of a novel heterohexanuclear complex of a pyrroloquinolinequinone (PQQ) derivative. In the crystal structure, two of the $Ru^{II}Ag^{I}$ heterodinuclear PQQ complexes were linked by two $[Ag^{I}(OTf)_2]^-$ units (OTf = $CF_3SO_3^-$) to form a unique hexanuclear structure. A solvent-bound $Ru^{II}Ag^{I}$ heterodinuclear complex was formed from the heterohexanuclear complex in a coordinating solvent such as acetone to show an intense metal-to-ligand charge-transfer band at 709 nm.

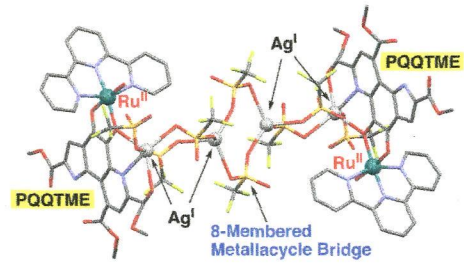

2277 S dx.doi.org/10.1021/ic302685h

Porphyrin-Substituted H-NOX Proteins as High-Relaxivity MRI Contrast Agents

Michael B. Winter, Piper J. Klemm, Christine M. Phillips-Piro, Kenneth N. Raymond, and Michael A. Marletta*

A highly thermally stable heme protein scaffold is evaluated as an MRI contrast agent. The native heme cofactor of the protein is substituted with manganese(II/III) and gadolinium(III) porphyrins for an improved MRI signal. The protein complexes are stable under aqueous conditions and display enhanced T_1 and T_2 relaxivities compared to commercial small-molecule agents.

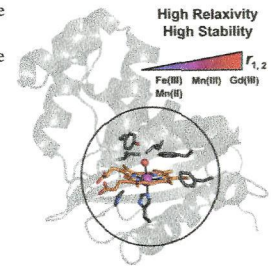

2280 S dx.doi.org/10.1021/ic302720d

Fabrication of Ruthenium Metal Nanosheets via Topotactic Metallization of Exfoliated Ruthenate Nanosheets

Katsutoshi Fukuda,* Jun Sato, Takahiro Saida, Wataru Sugimoto,* Yasuo Ebina, Tatsuo Shibata, Minoru Osada, and Takayoshi Sasaki

Ruthenium metal nanosheets with a two-dimensional hexagonal symmetry were fabricated via topotactic metallizatoin of exfoliated oxide nanosheets, which would be promising for device and catalysis applications as a new class of versatile nanometals.

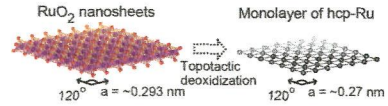

2283 S dx.doi.org/10.1021/ic3027368

Heptacoordinated Nickel(II) as an Ising-Type Anisotropic Building Unit: Illustration with a Pentanuclear $[(NiL)_3\{W(CN)_8\}_2]$ Complex

Nayanmoni Gogoi, Mehrez Thlijeni, Carine Duhayon, and Jean-Pascal Sutter*

A pentanuclear cyano-bridged $[Ni_3W_2]$ complex involving heptacoordinated nickel is found to exhibit single-molecule-magnet-type behavior.

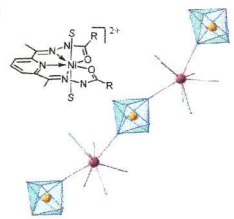

2286 S dx.doi.org/10.1021/ic302740j

Carbonate-Templated Self-Assembly of an Alkylthiolate-Bridged Cadmium Macrocycle

Wei Lai, Steven M. Berry, William P. Kaplan, Malia S. Hain, John C. Poutsma, Raymond J. Butcher, Robert D. Pike, and Deborah C. Bebout*

In the presence of $Cd(ClO_4)_2$, a new multidentate ligand supported both carbonate formation from atmospheric CO_2 and the self-assembly of a novel bis(carbonate)-capped puckered $(CdS)_6$ molecular wheel. The remarkable stability of the complex was investigated by ^1H NMR and electrospray ionization mass spectrometry.

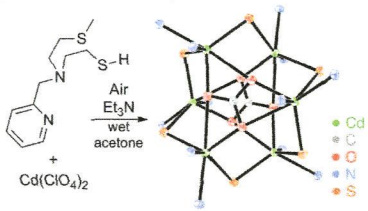

2289 S dx.doi.org/10.1021/ic3027946

Novel Hexanuclear Copper(II) Complex Built from a Simple Tetrachelating Triazole Ligand: Synthesis, Structure, and Magnetism

J. Hernández-Gil, N. Ovèjak, S. Ferrer,* F. Lloret, and A. Castiñeiras

A new easy symmetric 3,5-disubstituted 1,2,4-triazole ligand (H_3diV) by reaction with an excess of copper(II) salt has afforded a novel hexanuclear compound, which exhibits two types of Cu^{II} centers and two clearly distinguishable antiferromagnetic J_1 (-234 cm^{-1}) and J_2 (-35 cm^{-1}) coupling constants

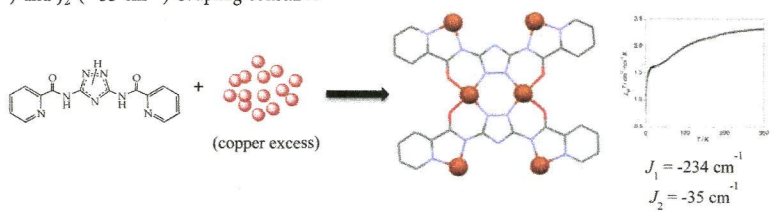

Articles

2292 S dx.doi.org/10.1021/ic300979cInvalid character: '^' [^], found in tag <document-title>. Context: ...xes with P>^<N Ligands ... . Possible substitution: ^ [̂]

Synthesis, Structure, and Characterization of Dinuclear Copper(I) Halide Complexes with P^N Ligands Featuring Exciting Photoluminescence Properties

Daniel M. Zink, Michael Bächle, Thomas Baumann,* Martin Nieger, Michael Kühn, Cong Wang, Wim Klopper, Uwe Monkowius,* Thomas Hofbeck, Hartmut Yersin,* and Stefan Bräse*

Invalid character: '^' [^], found in tag <synopsis>. Context: ...identate P>^<N ligands.... . Possible substitution: ^ [̂]

A series of highly luminescent dinuclear copper(I) complexes has been synthesized using a modular approach based on bidentate P^N ligands. Electron donors or acceptors as substituents on the ligand have been used to shift the LUMO of the complex in order to tune the emission across the whole visible range from 481 to 713 nm. Structures have been determined by X-ray analysis, and photophysical interpretations are supported by theoretical calculations. For a representative compound it is shown that the ambient-temperature emission represents a thermally activated delayed fluorescence.

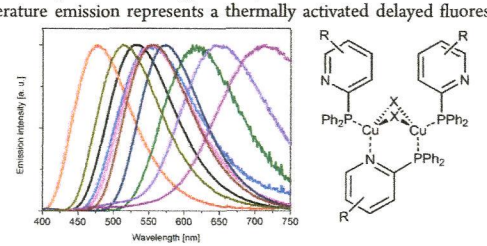

2306 S dx.doi.org/10.1021/ic301555r

Highly Sensitive and Selective Difunctional Ruthenium(II) Complex-Based Chemosensor for Dihydrogen Phosphate Anion and Ferrous Cation

Ze-Bao Zheng, Zhi-Ming Duan, Ying-Ying Ma, and Ke-Zhi Wang*

$[Ru(bpy)_2(Htppip)](ClO_4)_2$ acts as an efficient "turn on" luminescence sensor for $H_2PO_4^-$ in CH_3CN and CH_3CN/H_2O (50:1 v/v) solutions. In both the CH_3CN and aqueous 4-(2-hydroxyethyl)-1-piperazineethanesulfonic acid buffer (pH = 7.2)/CH_3CN (71/1, v/v) solution, it also exhibited a colorimetric sensing ability for Fe^{2+} through an obvious color change from pale yellow to light red-purple.

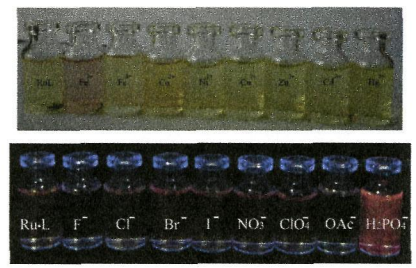

2317 S dx.doi.org/10.1021/ic301629m

Understanding Pd–Pd Bond Length Variation in (PNP)Pd–Pd(PNP) Dimers

Justin R. Walensky, Claudia M. Fafard, Chengyun Guo, Christina M. Brammell, Bruce M. Foxman, Michael B. Hall,* and Oleg V. Ozerov*

Dimeric (PNP)Pd–Pd(PNP) compounds display unexpectedly dramatic differences in the Pd–Pd bond lengths and overall symmetry as a function of seemingly minute changes in the supporting PNP pincer ligand. Analysis of the experimental and computational structures suggests that the intrinsic electronic preference for a symmetric dimer with a short Pd–Pd bond is *finely balanced with the steric encumbrance of bringing to (PNP)Pd fragments close.*

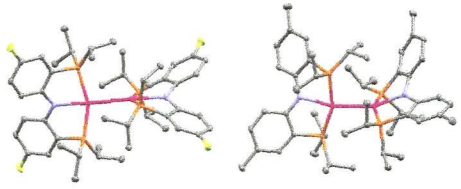

2323 S dx.doi.org/10.1021/ic301730z

Synthesis and Properties of Arsenic(III)-Reactive Coumarin-Appended Benzothiazolines: A New Approach for Inorganic Arsenic Detection

Vivian C. Ezeh and Todd C. Harrop*

A series of As-reactive benzothiazolines termed ArsenoFluors (AFs) have been synthesized and characterized. These constructs report subppb levels of As^{3+} via a 20–25 fluorescence turn-ON by forming the corresponding benzothiazoles.

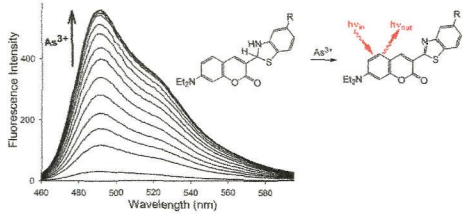

2335 S dx.doi.org/10.1021/ic301828e

Reduction and Protonation of Mo(IV) Imido Complexes with depe Coligands: Generation and Reactivity of a *S* = 1/2 Mo(III) Alkylnitrene Intermediate

Ameli Dreher, Sven Meyer, Christian Näther, Anne Westphal, Henning Broda, Biprajit Sarkar, Wolfgang Kaim, Philipp Kurz,* and Felix Tuczek*

Electro- and spectroelectrochemical investigations of $[Mo^{IV}(NEt)(CH_3CN)(depe)_2](OTf)_2$ (**2**-MeCN) presented in this study lead to generation of the Mo(III) alkylnitrene intermediate $[Mo^{III}(NEt)(CH_3CN)(depe)_2]OTf$ (**5**), which is immediately protonated to **5**H and then further reduced to $[Mo^{II}(HNEt)(CH_3CN)(depe)_2]OTf$ (**7**). The results support the central paradigm of alternating single reduction and protonation steps in the Schrock and Chatt cycles for biomimetic conversion of dinitrogen to ammonia.

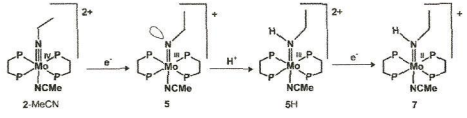

2353 S dx.doi.org/10.1021/ic301857h

A Porous 4-Fold-Interpenetrated Chiral Framework Exhibiting Vapochromism, Single-Crystal-to-Single-Crystal Solvent Exchange, Gas Sorption, and a Poisoning Effect

Ming-Hua Zeng,* Yan-Xi Tan, Yan-Ping He, Zheng Yin, Qing Chen, and Mohamedally Kurmoo*

A 4-fold-interpenetrated pseudodiamond framework, $Co^{II}(pybz)_2 \cdot 2DMF$, and its desolvated form $Co^{II}(pybz)_2$, possessing 47.0% void volume, can realize guest exchange in a single-crystal-to-single-crystal fashion. The as-synthesized crystals show an interesting color change from claret red to light pink upon exposure to water, which was associated with a water-induced change of coordination of the metal nodes. Tests show that $Co^{II}(pybz)_2$ may be a more efficient drying agent than silica gel and anhydrous $CuSO_4$. The desolvated $Co^{II}(pybz)_2$ can absorb several gases and organic vapors. In contrast, if $Co^{II}(pybz)_2$ is exposed to air followed by reactivation, its sorption capacity is considerably reduced because of a poisoning effect.

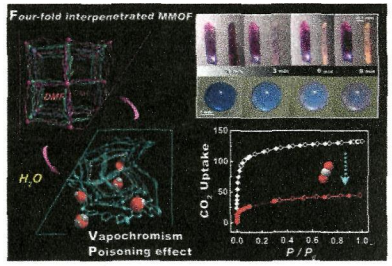

2361 S dx.doi.org/10.1021/ic301829x

Organometallic Oligomers Based on Bis(arylacetylide)bis(P-chirogenic phosphine)platinum(II) Complexes: Synthesis and Photonic Properties

Antony Lapprand, Naïma Khiri, Daniel Fortin, Sylvain Jugé,* and Pierre D. Harvey*

Oligomers of the type $(—C{\equiv}C—\mathbf{aryl}—C{\equiv}C—PtL_2—)_n$ [L = (*R*)- and (*S*)-P(Ph)(*i*Pr)($C_{17}H_{35}$); **aryl** = 1,4-benzene, 2,1,3-benzothiadiazole] exhibit a P-chiral environment that is modestly felt by the aryl moieties. These P($C_{17}H_{35}$)(Ph)(*i*-Pr)-containing materials exhibit red-shifted absorptions and emissions with respect to those including the PBu_3 ligands. The presence of the $C_{17}H_{35}$ chain does not greatly alter the τ_e, and fast T_1 energy transfer [terminal*] → [central] unit was deduced from the absence of luminescence arising from the terminal units.

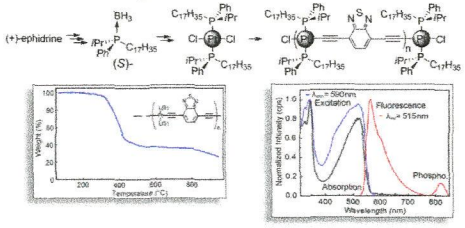

2372 Ⓢ dx.doi.org/10.1021/ic301889e

Electronic Structure and Spectroscopic Properties of Mononuclear Manganese(III) Schiff Base Complexes: A Systematic Study on [Mn(*acen*)X] Complexes by EPR, UV/vis, and MCD Spectroscopy (X = Hal, *NCS*)

Anne Westphal, Arne Klinkebiel, Hans-Martin Berends, Henning Broda, Philipp Kurz, and Felix Tuczek*

In the low-temperature MCD spectra of the [Mn(*acen*)X] complexes (H_2*acen*: *N*,*N*′-ethylenebis(acetyl-acetone)imine, X: I^-, Br^-, Cl^-, NCS^-) a "double *pseudo-A* term" is observed between 25000 and 35000 cm^{-1}. Based on MO and symmetry considerations, these features are assigned to $\pi^{n.b.}(s, a) \rightarrow yz, z^2$ ligand-to-metal charge transfer transitions. The observed sign change is explained by an inversion of symmetry among the $\pi^{n.b.}(s, a)$ donor orbitals which leads to an interchange of the positive and negative *pseudo-A* terms constituting the "double *pseudo-A* term".

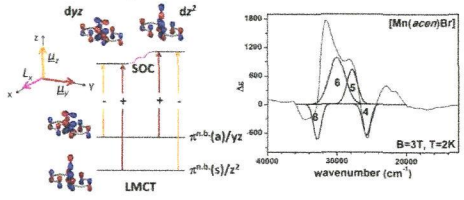

2388 Ⓢ dx.doi.org/10.1021/ic302047z

On the Structure of α-$BiFeO_3$

Hui Wang, Chengxu Yang, Jun Lu, Meimei Wu, Jie Su, Kuo Li, Junrong Zhang, Guobao Li,* Tounan Jin,* Takashi Kamiyama, Fuhui Liao, Jianhua Lin,* and Yicheng Wu

α-$BiFeO_3$ is confirmed to crystallize in the space group *P*1 with $a \approx 0.563\,44$ nm, $b \approx 0.563\,70$ nm, $c \approx 0.563\,63$ nm, $\alpha \approx 59.32°$, $\beta \approx 59.36°$, $\gamma \approx 59.33°$, and the magnetic structure of α-$BiFeO_3$ can be described by the space group *P*1 with a magnetic modulation vector in reciprocal space $\mathbf{q} = 0.0045\mathbf{a}^* - 0.0045\mathbf{b}^*$.

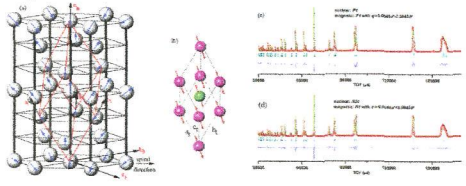

2393 Ⓢ dx.doi.org/10.1021/ic302100x

NMR Investigation of the Spontaneous Thermal- and/or Photoinduced Reduction of trans Dihydroxido Pt(IV) Derivatives

Emanuele Petruzzella, Nicola Margiotta,* Mauro Ravera, and Giovanni Natile*

[$PtCl_2$(*cis*-1,4-DACH)] (Kiteplatin, **1**; DACH = diaminocyclohexane) was oxidized with H_2O_2 to afford *cis,trans,cis*-[$PtCl_2(OH)_2$(*cis*-1,4-DACH)] (**2**) which was further derivatized with succinic anhydride. To our surprise, in DMF (50−70 °C or under light irradiation) or in DMSO (under light irradiation) the formation of the succinato complex *cis,trans,cis*-[$PtCl_2${$OC(O)CH_2CH_2C(O)OH$}$_2$(*cis*-1,4-DACH)] (**3**) was accompanied by reduction to **1**. The mechanism involves solvolysis of **2** and formation of a μ-oxo dinuclear species (**5**) that can then undergo reduction to a 1:1 mixture of **1** and **2** with concomitant elimination of oxygen (1/2 O_2 in the form of H_2O_2).

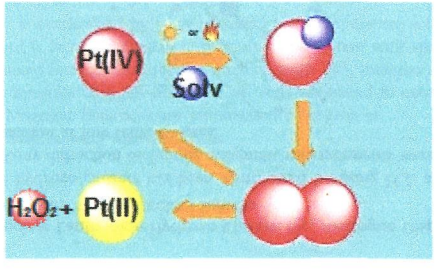

2404 dx.doi.org/10.1021/ic302168g

Excess Heat Capacity in Liquid Binary Alkali-Fluoride Mixtures

M. Beilmann, O. Beneš,* E. Capelli, V. Reuscher, R. J. M. Konings, and Th. Fanghänel

Enthalpy increments were measured for the liquid state of the LiF−KF, LiF−RbF, and LiF−CsF binary systems, using drop calorimetry. From the obtained results, the excess heat capacities were derived for the entire composition ranges and compared with the LiF−NaF system. A clear tendency was found that the excess heat capacities depend on the cation radii of the salt melt and increase in the following order: LiF−NaF < LiF−KF < LiF−RbF < LiF−CsF.

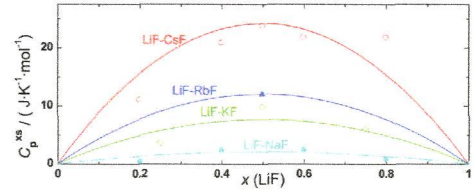

2412 Ⓢ dx.doi.org/10.1021/ic302180t

Formation of a Metal-to-Nitrogen Bond of Normal Length by a Neutral Sufonamide Group within a Tridentate Ligand. A New Approach to Radiopharmaceutical Bioconjugation

Theshini Perera, Pramuditha Abhayawardhana, Patricia A. Marzilli, Frank R. Fronczek, and Luigi G. Marzilli*

We demonstrate that a tertiary sulfonamide group, R'_2NSO_2R, can rehybridize to form a M−N bond of normal length even when that group is in a linear tridentate ligand, such as the new tridentate $N(SO_2R)$dpa ligands derived from di-(2-picolyl)amine (N(H)dpa). The new *fac*-[$Re(CO)_3(N(SO_2R)$dpa)]X structures provide the only examples for any metal with the sulfonamide as part of a noncyclic linear tridentate ligand and with a normal metal-to-nitrogen(tertiary sulfonamide) bond length.

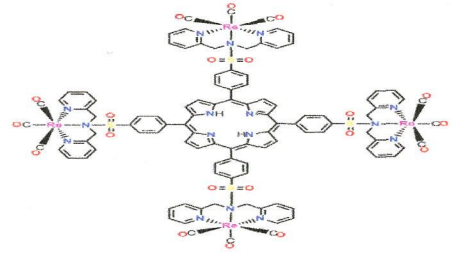

2422 Ⓢ dx.doi.org/10.1021/ic3022672

Effect of d-Amino Acid Substitutions on Ni(II)-Assisted Peptide Bond Hydrolysis

Hanieh H. Ariani, Agnieszka Polkowska-Nowakowska, and Wojciech Bal*

Sequence-specific Ni(II)-dependent peptide bond hydrolysis is extremely sensitive not to the absolute but to the relative side chain orientation in the active complex. The main 5 influential amino acids (SRHWK) in the square planar Ni(II) complex of previously defined sequence Ac-GASRHWKFL-NH_2 were substituted with d-amino acids one by one. Each new analogue implies new information about the precise cooperation among the amino acid side chains.

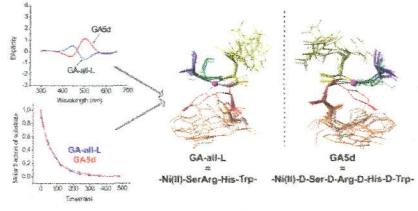

2432 S dx.doi.org/10.1021/ic3022886

New Structural Form of a Tetranuclear Lanthanide Hydroxo Cluster: Dy_4 Analogue Display Slow Magnetic Relaxation

Ananda Kumar Jami, Viswanathan Baskar,* and E. Carolina Sañudo

A series of tetranuclear lanthanide hydroxo clusters has been synthesized by using H_3L as ligand. The solid state structures were established by single crystal X-ray diffraction technique. Magnetic measurements were carried out for **1**−**3**, of which Dy_4 cluster exhibits slow magnetic relaxation at low temperatures.

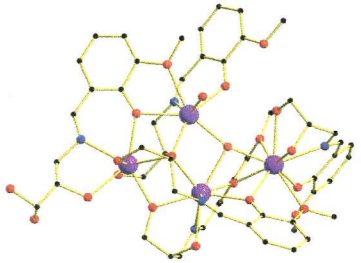

2439 S dx.doi.org/10.1021/ic302297u

One-Pot Syntheses and Cell Imaging Applications of Poly(amino acid) Coated $LaVO_4$:Eu^{3+} Luminescent Nanocrystals

Huanjie Wang and Leyu Wang*

Water-stable, bioconjugatable, and luminescent poly(amino acid) coated $LaVO_4$:Eu^{3+}−PASP nanoparticles have been successfully prepared via a green and facile one-pot strategy and applied for cell imaging.

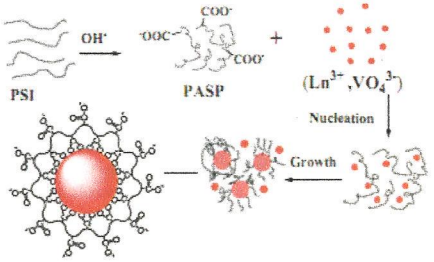

2446 S dx.doi.org/10.1021/ic302320w

Synthesis of a Bis(indenyl) Co(I) Anion: A Reactive Source of a 14 Electron Indenyl Co(I) Equivalent

Fernando Hung-Low and Christopher A. Bradley*

Bis(indenyl) cobaltate anion $[Na(THF)_6][(\eta^5\text{-}C_9H_5\text{-}1,3\text{-}(SiMe_3)_2)_2Co]$ (**2**) has been prepared by reduction of the corresponding bis(indenyl) cobalt(II) complex and characterized by both structural and reactivity studies. Complex **2** displays reactivity consistent as a source of an (indenyl)Co(I) equivalent, as addition of σ or π donors to **2** results in the extrusion of indenide ligand and formation of (indenyl)CoL_n ligand adducts. Complex **2** represents an elusive intermediate from analogous cobaltocene chemistry utilized in the generation of CpCo(I) fragments for small molecule activation.

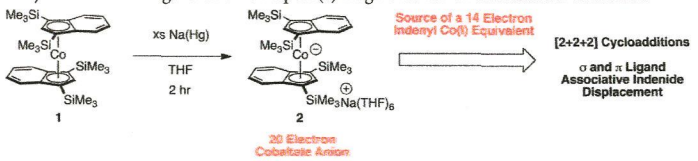

2458 S dx.doi.org/10.1021/ic3023503

X_2Y_2 Isomers: Tuning Structure and Relative Stability through Electronegativity Differences (X = H, Li, Na, F, Cl, Br, I; Y = O, S, Se, Te)

Majid El-Hamdi, Jordi Poater,* F. Matthias Bickelhaupt,* and Miquel Solà*

The Y−Y bond length of the XYYX and X_2YY isomers (Y = O, S, Se, Te) can be tuned quite generally through the X−Y electronegativity difference. The mechanism behind this electronic tuning is the population or depopulation of the π^* in the YY fragment.

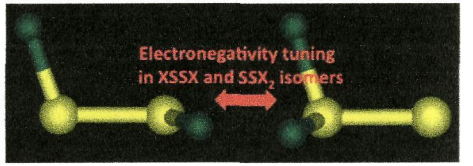

2466 S dx.doi.org/10.1021/ic302357h

New Fluoride Carbonates: Centrosymmetric $KPb_2(CO_3)_2F$ and Noncentrosymmetric $K_{2.70}Pb_{5.15}(CO_3)_5F_3$

T. Thao Tran and P. Shiv Halasyamani*

Two new potassium lead fluoride carbonates, $KPb_2(CO_3)_2F$ and $K_{2.70}Pb_{5.15}(CO_3)_5F_3$, have been synthesized and characterized. Both materials exhibit two-dimensional layered structures. $KPb_2(CO_3)_2F$ consists of double-layers of $Pb(CO_3)_3F$ polyhedra, whereas $K_{2.70}Pb_{5.15}(CO_3)_5F_3$ consists of double-layers of $Pb(CO_3)_3F$ polyhedra alternating with triple-layers of $Pb(CO_3)_3F$−$Pb(CO_3)_3F_2$−$Pb(CO_3)_3F$ polyhedra. $K_{2.70}Pb_{5.15}(CO_3)_5F_3$ is noncentrosymmetric, and crystallizes in the *achiral* and *nonpolar* space group $P\bar{6}m2$. The intrinsically asymmetric structures of the double and triple-layers in $KPb_2(CO_3)_2F$ and $K_{2.70}Pb_{5.15}(CO_3)_5F_3$ make a positive contribution to noncentrosymmetric material engineering.

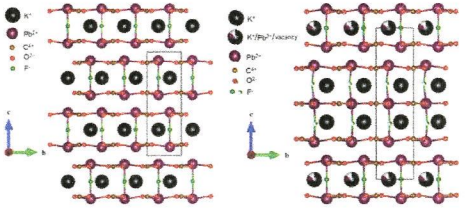

$KPb_2(CO_3)_2F$ $K_{2.70}Pb_{5.15}(CO_3)_5F_3$

2474 S dx.doi.org/10.1021/ic302380z

Gold(III) Porphyrins Containing Two, Three, or Four β,β'-Fused Quinoxalines. Synthesis, Electrochemistry, and Effect of Structure and Acidity on Electroreduction Mechanism

Zhongping Ou,* Tony Khoury, Yuanyuan Fang, Weihua Zhu, Paul J. Sintic, Maxwell J. Crossley,* and Karl M. Kadish*

Gold(III) porphyrins containing three and four β,β'-fused quinoxalines were synthesized and examined as to their electrochemical properties in nonaqueous media containing added acid. The initial $Au(PQ_3)PF_6$ compound is shown to undergo a total of four Au^{III}/Au^{II} processes while $Au(PQ_4)PF_6$ exhibits five metal-centered one-electron reductions prior to the occurrence of additional reductions at the conjugated macrocycle and fused quinoxaline rings in acidic solutions. An overall mechanism for reduction in nonaqueous media with and without added acid is proposed.

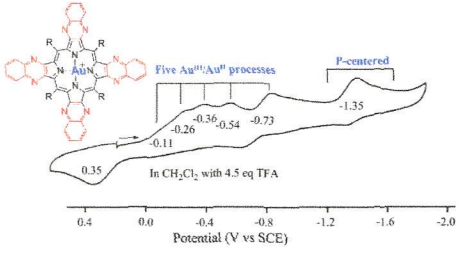

2484 S dx.doi.org/10.1021/ic302391u

Manganese as a Substitute for Rhenium in CO_2 Reduction Catalysts: The Importance of Acids

*Jonathan M. Smieja, Matthew D. Sampson, Kyle A. Grice, Eric E. Benson, Jesse D. Froehlich, and Clifford P. Kubiak**

Electrocatalytic properties, X-ray crystallographic studies, and infrared spectroelectrochemistry (IR-SEC) of Mn(bpy-*t*Bu)$(CO)_3$Br, an electrocatalyst for the reduction of CO_2 to CO, are reported. Unlike the analogous rhenium catalyst, the addition of Brönsted acids to CO_2-saturated solutions is necessary for catalytic turnover. This manganese catalyst reduces CO_2 with similar activities and operates at a lower overpotential as compared with its rhenium analogue. X-ray crystallography of the reduced species, $[Mn(bpy\text{-}tBu)(CO)_3]^-$, shows a five-coordinate Mn center, similar to its rhenium analogue.

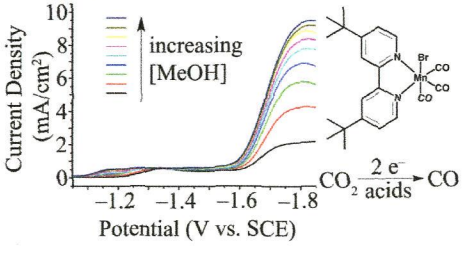

2492 S dx.doi.org/10.1021/ic3023979

Synthesis and Magnetic Properties of a New Borophosphate $SrCo_2BPO_7$ with a Four-Column Ribbon Structure

Wenbin Gou, Zhangzhen He,* Ming Yang, Weilong Zhang, and Wendan Cheng

A new borophosphate $SrCo_2BPO_7$ is synthesized by a conventional high-temperature solid-state reaction. The titled compound is found to crystallize in monoclinic system with space group $P2_1/c$, which displays a distorted four-column ribbon structure. Both BO_3 triangles and PO_4 tetrahedra are isolated, while irregular triangles built by Co^{2+} ions are found to exist between the connecting ribbons. Magnetic behaviors are investigated by means of susceptibility, magnetization, and heat capacity measurements.

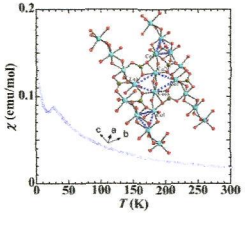

2497 S dx.doi.org/10.1021/ic302444b

Removal of Mercury from the Environment: A Quantum-Chemical Study with the Normalized Elimination of the Small Component Method

Wenli Zou, Michael Filatov, David Atwood, and Dieter Cremer*

Strongly chelating organic compounds ("organic tweezers") can react with Hg ions in aqueous solution to form precipitates, which can be mechanically removed from the solution. The structure and stability of 1,3-benzenediamidoethanethiolate-mercury and its selenium and tellurium analogues are investigated with the Dirac exact relativistic normalized elimination of the small component method to determine the usefulness of the organic tweezers compound 1,3-benzenediamidoethanethiol for cleaning up the environment from mercury.

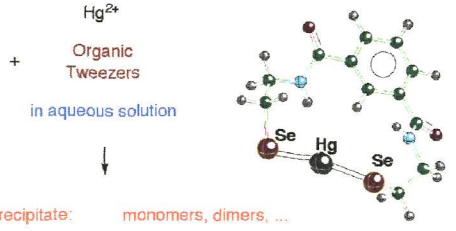

2505 S dx.doi.org/10.1021/ic302446h

Catalytic Water Oxidation by Mononuclear Ru Complexes with an Anionic Ancillary Ligand

Lianpeng Tong, A. Ken Inge, Lele Duan, Lei Wang, Xiaodong Zou, and Licheng Sun*

Two mononuclear Ru complexes were prepared and fully characterized. Both of them show impressive activity for catalytic water oxidation. The catalytic mechanism and effect of ancillary ligands were discussed based on the two candidates in the context of catalytic water oxidation.

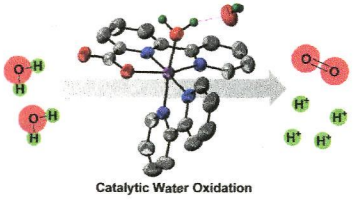

2519 dx.doi.org/10.1021/ic302457m

High-Temperature X-ray Diffraction Study of Uranium–Neptunium Mixed Oxides

Mélanie Chollet, Renaud C. Belin,* Jean-Christophe Richaud, Muriel Reynaud, and Frédéric Adenot

We describe for the first time the oxidation of $(U_{1-y}Np_y)O_2$ oxides up to 1373 K with in situ X-ray diffraction (XRD). First, we highlight the limited knowledge on Np–O and U–Np–O compared to U–O. Then, by analyzing in situ XRD patterns during the oxidation sequence of stoichiometric materials, we discuss the observed phase relationships and compare them to that found in similar systems such as U–Pu–O.

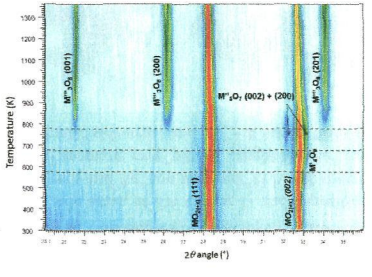

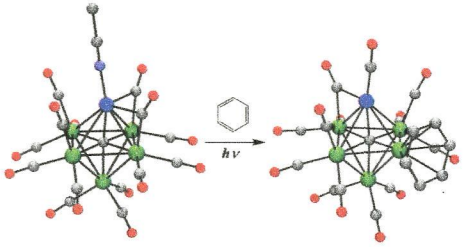

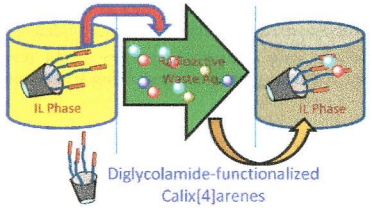

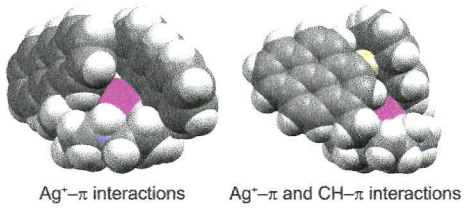

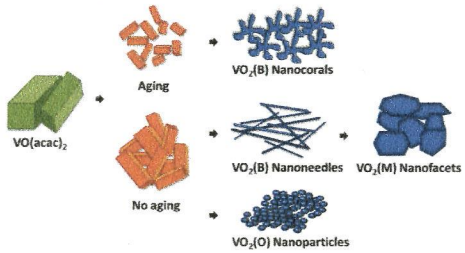

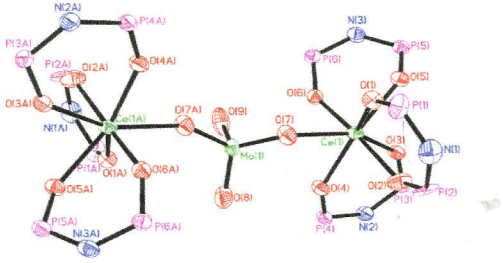

2564 S dx.doi.org/10.1021/ic302570s

Guanidinato Complexes of Iridium: Ligand-Donor Strength, O_2 Reactivity, and (Alkene)peroxoiridium(III) Intermediates

Matthew R. Kelley and Jan-Uwe Rohde*

Monoanionic guanidinato ligands facilitate oxygen activation at iridium, leading to the accumulation of (alkene)peroxo intermediates prior to alkene oxygenation. Control of the reactivity is achieved by subtle tuning of ligand sterics that allows switching between irreversible and reversible binding of O_2.

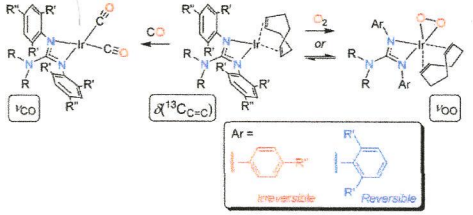

2581 S dx.doi.org/10.1021/ic302585g

Self-Assembly of Three-Dimensional $SrTiO_3$ Microscale Superstructures and Their Photonic Effect

Xiaoliang Yuan, Maojun Zheng,* Yafeng Zhang, Tao Zhou, Changli Li, Xiaosheng Fang, Li Ma, and Wenzhong Shen

3D STOMSs have been prepared *via* hydrothermal synthesis and multiple (five times) crystallization process. Branches and trunks on STOMSs show perfect corn-like structures, and each side of the trunks could be considered as grating-analogous structures. These well-ordered trunks along with gratings constitute 3D hybrid microstructures that contribute to light diffraction, and the colorful photonic effects of light diffraction are thought to be due to refractive index modulations in three dimensions.

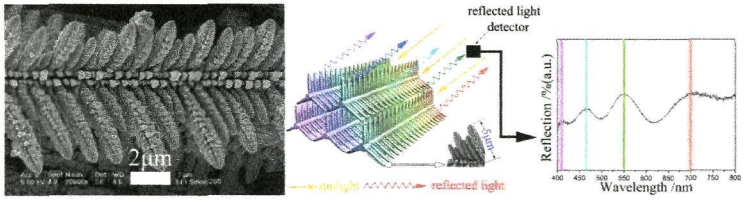

2588 S dx.doi.org/10.1021/ic302614k

Syntheses, Structures, and Magnetic Properties of a Family of Heterometallic Heptanuclear $[Cu_5Ln_2]$ (Ln = Y(III), Lu(III), Dy(III), Ho(III), Er(III), and Yb(III)) Complexes: Observation of SMM behavior for the Dy(III) and Ho(III) Analogues

Vadapalli Chandrasekhar,* Atanu Dey, Sourav Das, Mathieu Rouzières, and Rodolphe Clérac*

The reaction of a multisite coordination ligand (LH_3) with $Cu(OAc)_2{\cdot}H_2O$ and a rare-earth(III) nitrate salt in the presence of triethylamine afforded a series of heterometallic heptanuclear complexes containing a $[Cu_5Ln_2]$ core {Ln = Y(**1**), Lu(**2**), Dy(**3**), Ho(**4**), Er(**5**), and Yb(**6**)}. Detailed static and dynamic magnetic properties of all the complexes have been studied and revealed the single-molecule magnet behavior of the Dy(III) and Ho(III) derivatives.

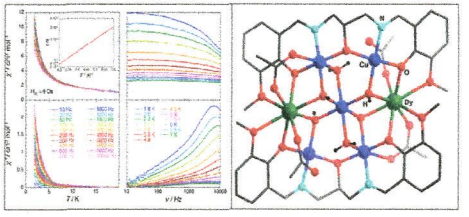

2599 S dx.doi.org/10.1021/ic302631d

Copper(II) Thiaethyneporphyrin and Copper(II) 21-Phosphoryl N-confused Porphyrin Hybrids. Intramolecular Copper(II)–Carbon Interaction Inside of a Porphyrinoid Surrounding

Norbert Grzegorzek, Elżbieta Nojman, Ludmiła Szterenberg, and Lechosław Latos-Grażyński*

Stabilization of organocopper(II) species has been achieved via the very efficient protection of copper(II)–carbon bond encapsulated in a coordination core of suitably constructed carbaporphyrinoids, trapping appropriately copper(II) η^1-C side-on (left) or equatorial copper(II)$\cdots\eta^2$-CC (right) structural motifs.

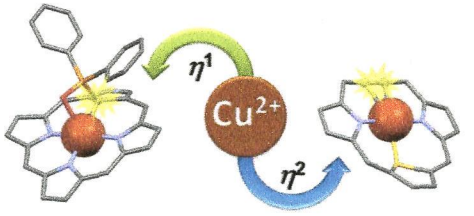

2607 S dx.doi.org/10.1021/ic302633y

Synthesis and Structural Analysis of (Imido)Vanadium(V) Complexes Containing Chelate (Anilido)Methyl-imine Ligands: Ligand Effect in Ethylene Dimerization

Kotohiro Nomura,* Atsushi Igarashi, Shohei Katao, Wenjuan Zhang, and Wen-Hua Sun

Syntheses and some structural analyses of $VCl_2(L)(NR)$ [R = 1-adamantyl, L = 2-(2,6-$Me_2C_6H_3$)$NCH_2(C_9H_6N)$, 8-(2,6-$Me_2C_6H_3$)$NCH_2(C_9H_6N)$; L = 2-(2,6-$R'_2C_6H_3$)$NCH_2(C_5H_4N)$, R = 2-MeC_6H_4 (**4**), 4-MeC_6H_4 (**5**), 3,5-$Me_2C_6H_3$ (**6**)], and their use as the catalyst precursor in the reactions with ethylene in the presence of MAO have been explored. The reactions with ethylene by **4**–**6** afforded 1-butene with high selectivities (>92%): **4** (R′ = Me, ^{i}Pr) exhibited superior activities and selectivity in ethylene dimerization.

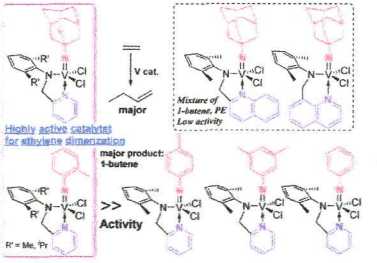

2615 dx.doi.org/10.1021/ic302662x

Thermal Response, Catalytic Activity, and Color Change of the First Hybrid Vanadate Containing Bpe Guest Molecules

Roberto Fernández de Luis, M. Karmele Urtiaga, José L. Mesa, Edurne S. Larrea, Marta Iglesias, Teófilo Rojo, and María I. Arriortua*

The $[\{Co_xNi_{2-x}(H_2O)_2(Bpe)_2(V_4O_{12})\}]\cdot 4H_2O$ Bpe, $x = 2, 1, 0.6, 0$, isomorphic compounds possess a three-dimensional crystal framework in which [001] channels are located in the Bpe guest molecules. The reversible loss/uptake of crystallization and coordinated water molecules gives rise to an appreciable color change, due to the distortion of the coordination environment of the Ni(II) and Co(II) metal centers.

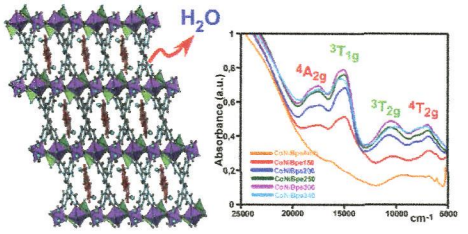

2627 dx.doi.org/10.1021/ic302543n

Factors Affecting the Carboxylate Shift Upon Formation of Nonheme Diiron-O_2 Adducts

Jonathan R. Frisch, Ryan McDonnell, Elena V. Rybak-Akimova,* and Lawrence Que Jr.*

$[Fe^{II}_2(N\text{-EtHPTB})(O_2CR)]^{2+}$ complexes react with O_2 at −90 °C to form blue-green adducts ($\mathbf{2}\cdot O_2CR$) that convert readily and irreversibly to blue $\mathbf{3}\cdot O_2CR$ isomers due to the shift of the carboxylate ligand from a bridging mode in $\mathbf{2}\cdot O_2CR$ to a terminal monodentate binding mode in $\mathbf{3}\cdot O_2CR$. The rate of this "carboxylate shift" is retarded by increasing the basicity of the XO_2 moiety, its steric bulk, and the O···O bite distance.

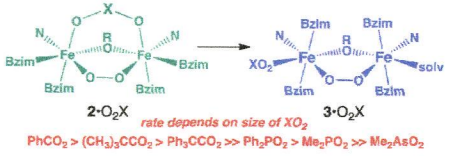

2637 dx.doi.org/10.1021/ic3026705

Synthesis, Structure, and Characterization of Two New Polar Sodium Tungsten Selenites: $Na_2(WO_3)_3(SeO_3)\cdot 2H_2O$ and $Na_6(W_6O_{19})(SeO_3)_2$

Sau Doan Nguyen and P. Shiv Halasyamani*

New polar $Na_2(WO_3)_3(SeO_3)\cdot 2H_2O$ ($P3_1c$) and $Na_6(W_6O_{19})(SeO_3)_2$ ($C2$) materials have been synthesized and characterized. $Na_2(WO_3)_3(SeO_3)\cdot 2H_2O$ exhibits a strong second-harmonic-generation efficiency attributable to a class 2 hexagonal tungsten oxide layered structure, whereas $Na_6(W_6O_{19})(SeO_3)_2$ exhibits a weak SHG efficiency because of two-fold rotation symmetry of the "ribbon". Both materials are piezoelectric and pyroelectric but are not ferroelectric.

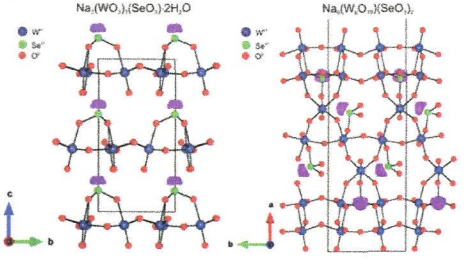

2648 dx.doi.org/10.1021/ic302674g

Synthesis and Disordered Crystal Structure of $Al_3O_{3.5}C_{0.5}$

Toru Asaka, Ryosuke Kotani, Tatsunari Kudo, Hideto Yoshida, and Koichiro Fukuda*

The structural model of $Al_3O_{3.5}C_{0.5}$ is determined by laboratory X-ray powder diffraction, which shows the positional disordering of one of the two types of Al sites. Under TEM, weak diffraction spots reveal a doubling of the a axis with respect to the hexagonal basic cell. The structural disordering is probably induced by the high-low phase transition.

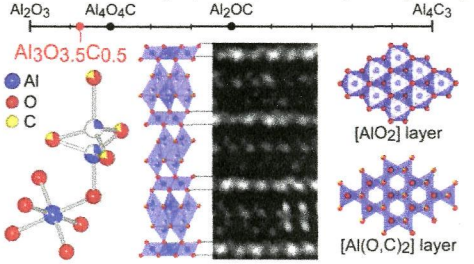

2654 dx.doi.org/10.1021/ic302682f

Step-by-Step Introduction of Silazane Moieties at Ruthenium: Different Extents of Ru−H−Si Bond Activation

Katharine A. Smart, Mary Grellier,* Laure Vendier, Sax A. Mason, Silvia C. Capelli, Alberto Albinati, and Sylviane Sabo-Etienne*

The elucidation of Si−H activation processes is crucial for accurate descriptions of catalytic hydrosilylation and functionalization of organosilanes. Stepwise incorporation of one, two, or three silazane ligands has enabled the preparation of novel mononuclear and dinuclear ruthenium compounds that exhibit an interesting range of multicenter Ru−H−Si interactions with varying degrees of Si−H activation.

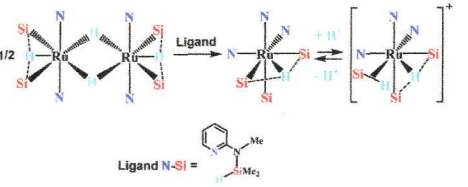

2662 dx.doi.org/10.1021/ic302703k

Synthesis and Structural Characterization of Inorganic-Organic-Inorganic Hybrids of Dipalladium-Substituted γ-Keggin Silicodecatungstates

Tomohisa Hirano, Kazuhiro Uehara, Sayaka Uchida, Mitsuhiro Hibino, Keigo Kamata, and Noritaka Mizuno*

Inorganic-organic-inorganic hybrids of dipalladium-substituted γ-Keggin silicodecatungstates, $TBA_8[\{(\gamma\text{-}H_2SiW_{10}O_{36}Pd_2)\text{-}(O_2C(CH_2)_nCO_2)\}_2]$ ($n = 1$ (**II**), 3 (**III**), and 5 (**IV**), (TBA = $[(n\text{-}C_4H_9)_4N]^+$)), were synthesized by exchange of the acetate ligands in $TBA_4[\gamma\text{-}H_2SiW_{10}O_{36}Pd_2(OAc)_2]$ and structurally characterized. The lengths between two polyoxometalates increased with increase in methylene chain lengths of organic linkers. The reversible structure transformation of **IV** driven by 1,2-dichloroethane sorption−desorption was investigated by the powder XRD measurements.

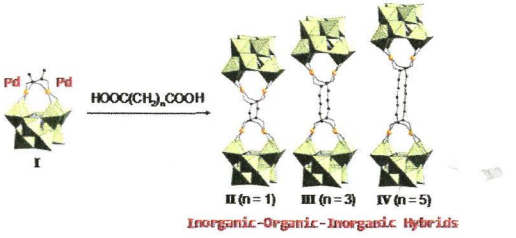

2671 S dx.doi.org/10.1021/ic301040d

Antiferromagnetic Spin Correlations Between Corner-Shared $[FeO_5]^{7-}$ and $[FeO_6]^{9-}$ Units, in the Novel Iron-Based Compound: $BaYFeO_4$

Friederike Wrobel, Moureen C. Kemei, and Shahab Derakhshan*

The crystal structure of the novel $BaYFeO_4$ is composed of alternate corner-shared units of $[FeO_5]^{7-}$ square pyramids (blue) and $[FeO_6]^{9-}$ octahedral (purple) in a stairwise arrangement, resulting in one-dimensional channels. The Fe^{3+} ions are coupled antiferromagnetically and exhibit two transitions at 33 and 48 K in temperature-dependent magnetic susceptibility data.

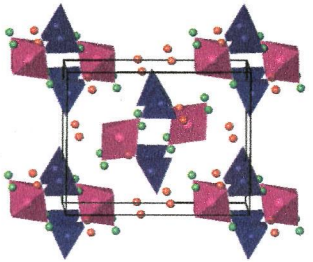

2678 S dx.doi.org/10.1021/ic302727w

Structural Diversity in Alkali Metal Complexes of Sterically Demanding Carbazol-9-yl Ligands

Rhiannon S. Moorhouse, Graeme J. Moxey, Fabrizio Ortu, Thomas J. Reade, William Lewis, Alexander J. Blake, and Deborah L. Kays*

The sterically demanding 1,3,6,8-tetra-*tert*-butylcarbazol-9-yl ($^tBu_4carb^-$) ligand has been used to stabilize amide complexes of lithium, sodium, and potassium. Dimeric lithium complex $[^tBu_4carbLi]_2$ features a planar LiNLiN rhomboid ring. Recrystallization of the lithium, sodium, and potassium complexes from THF leads to the formation of $^tBu_4carbLi(THF)_2$, $^tBu_4carbNa(THF)_3$, and $^tBu_4carbK(THF)_4$ in the solid state. As group 1 is descended, there is an increase in hapticity of the binding of the ligands to the metal cations of the adducts.

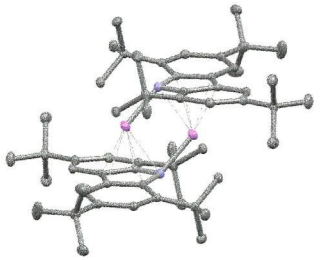

2684 S dx.doi.org/10.1021/ic302766f

Comparative Insight into Electronic Properties and Reactivities toward C–H Bond Activation by Iron(IV)–Nitrido, Iron(IV)–Oxo, and Iron(IV)–Sulfido Complexes: A Theoretical Investigation

Hao Tang, Jia Guan, Huiling Liu,* and Xuri Huang*

A comparative study on the electronic properties and reactivity of iron(IV)–oxo, –sulfido, and –nitrido complexes as well as complexes with various axial ligands bound basing on DFT methods reveals that the iron(IV)–nitrido complexes are capable of hydroxylating C–H bond of methane as good as the iron(IV)–oxo and –sulfido counterparts, and the reactivity of iron(IV)–nitrido oxidants in the quintet state enhances as the electron-donating ability of the axial ligand weakens.

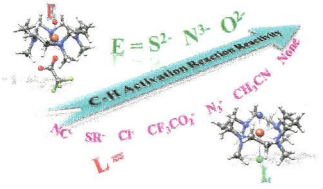

2697 S dx.doi.org/10.1021/ic302767b

Cluster Chemistry in Electron-Poor Ae–Pt–Cd Systems (Ae = Ca, Sr, Ba): $(Sr,Ba)Pt_2Cd_4$, $Ca_6Pt_8Cd_{16}$, and Its Known Antitype $Er_6Pd_{16}Sb_8$

Saroj L. Samal, Fakhili Gulo, and John D. Corbett*

Three new ternary polar intermetallic compounds, cubic $Ca_6Pt_8Cd_{16}$, and tetragonal (Sr, Ba)Pt_2Cd_4 have been discovered during explorations of the Ae–Pt–Cd systems. Cubic $Ca_6Pt_8Cd_{16}$ (*Fm*-3*m*, $Z = 4$, $a = 13.513(1)$ Å) contains a 3D array of separate Cd_8 tetrahedral stars (*TS*) that are both face capped along the axes and diagonally bridged by Pt atoms to generate the 3D anionic network $Cd_8[Pt(1)]_{6/2}[Pt(2)]_{4/8}$. The complementary cationic surface of the cell consists of a face-centered cube of Pt(3)@Ca_6 octahedra.

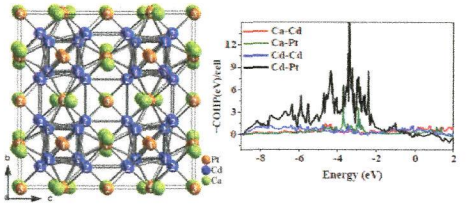

2705 S dx.doi.org/10.1021/ic302779q

Cancer Cell Cytotoxicity of Cyclometalated Compounds Obtained with Osmium(II) Complexes

Bastien Boff, Christian Gaiddon, and Michel Pfeffer*

The in vitro cytotoxicity (up to the nanomolar range) of 29 organometallic osmium derivatives against the A172 tumor cell line has been evaluated.

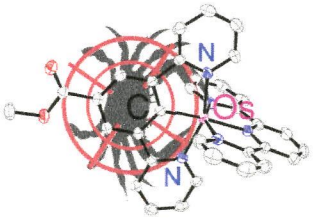

2716 S dx.doi.org/10.1021/ic3027978

Influence of Terminal Acryloyl Arms on the Coordination Chemistry of a Ditopic Pyrimidine–Hydrazone Ligand: Comparison of Pb(II), Zn(II), Cu(II), and Ag(I) Complexes

Daniel J. Hutchinson, Lyall R. Hanton,* and Stephen C. Moratti

Reacting a new pym–hyz ligand, containing terminal acryloyl arms, with excess amounts of Pb(II), Zn(II), Cu(II), and Ag(I) ions resulted in linear complexes, some of which showed coordination between the acryloyl arms and the metal ions. The presence of the acryloyl arms did influence the outcome of self-assembly on a 1:1 metal to ligand ratio, as mononuclear bent complexes were formed with Cu(II) and bent corner complexes were formed with Zn(II) ions.

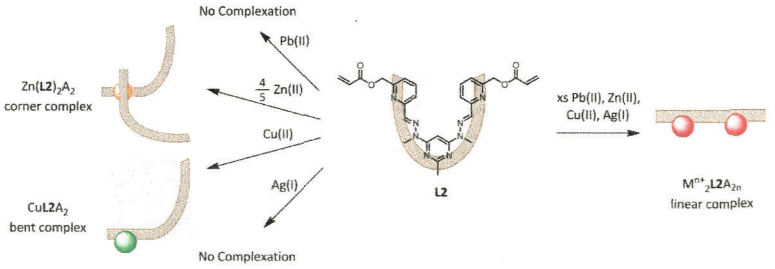

2729 S dx.doi.org/10.1021/ic302820z

Macrocyclization of the ATCUN Motif Controls Metal Binding and Catalysis

Kosh P. Neupane, Amanda R. Aldous, and Joshua A. Kritzer*

We report the design, synthesis, and characterization of macrocyclic analogues of the amino-terminal copper and nickel binding (ATCUN) motif. These macrocycles still bind Cu(II) and Ni(II) in a square planar geometry, but with altered thermodynamics of metal binding. Macrocyclization enhanced DNA cleavage by Cu(II)-peptide complexes, and the Cu(II)-macrocycle complex was also capable of producing diffusible hydroxyl radicals, which is unique among ATCUN motifs and most other common Cu(II) chelators.

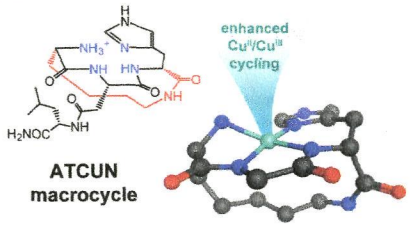

2736 S dx.doi.org/10.1021/ic302847g

Syntheses and Structures of a Series of Uranyl Phosphonates and Sulfonates: An Insight into Their Correlations and Discrepancies

Weiting Yang, Tao Tian, Hong-Yue Wu, Qing-Jiang Pan,* Song Dang, and Zhong-Ming Sun*

Six new uranyl phosphonates and sulfonats based on phenylphosphonic, 3- and 5-sulfoisophthalic acid and N-contained structure agents have been hydrothermally prepared. Secondary ligands tib, pi and dib play a crucial role in the formation of **UPhP-1**, **-2**, and **-3**. Sulfonate groups of 3- and 5-SP ligands exhibit unidentate coordination mode, and yield three different architectures of **USP-1**, **-2**, and **-3**.

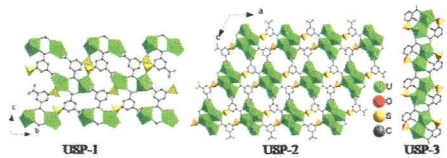

2744 S dx.doi.org/10.1021/ic302856b

Metal–Organic Frameworks as Hosts for Photochromic Guest Molecules

D. Hermann, H. Emerich, R. Lepski, D. Schaniel, and U. Ruschewitz*

Photoactive azobenzene was embedded in MOF-5, MIL-53(Al), MIL-68(Ga), and MIL-68(In). The trans → cis isomerization after illumination with UV light was followed by IR spectroscopy. An improved switching compared to pure azobenzene was observed for azobenzene$_5$@MOF-5, azobenzene$_{0.66}$@MIL-68(Ga), and azobenzene$_{0.66}$@MIL-68(In), but for azobenzene$_{0.5}$@MIL-53(Al), no switching was found. A structural analysis reveals that the size and the shape of the MOF's channels as well as the orientation of azobenzene within these channels are responsible for this different behavior.

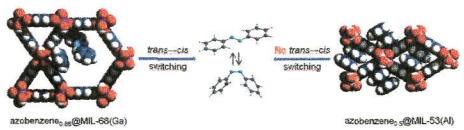

2750 S dx.doi.org/10.1021/ic4000389

Complexation of U(VI) with Dipicolinic Acid: Thermodynamics and Coordination Modes

Chao Xu, Guoxin Tian, Simon J. Teat, and Linfeng Rao*

UO_2^{2+} forms two successive complexes with dipicolinic acid (H_2L), $UO_2L(aq)$, and $UO_2L_2^{2-}$. The complexation in aqueous solutions is driven by both enthalpy and entropy. The exothermic enthalpy of complexation results from the participation of the pyridine nitrogen in the coordination and the optimal conjugated planar structure of the ligand that requires little preorganization energy.

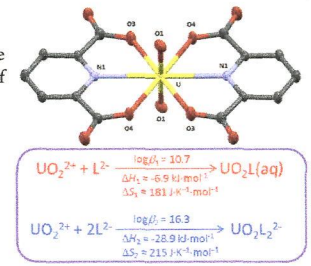

2757 S dx.doi.org/10.1021/ic400062b

Kinetics of Reduction of Aqueous Hexaammineruthenium(III) Ion at Pt and Au Microelectrodes: Electrolyte, Temperature, and Pressure Effects

Vijendran Vijaikanth, Guangchun Li, and Thomas W. Swaddle*

Rate constants obtained by impedance spectroscopy for the reduction of $Ru(NH_3)_6^{3+}$ at Au and Pt microelectrodes are strongly dependent on the total concentrations of the specific anion, and the corresponding volumes of activation are more negative than can be accommodated by theory successfully with other electron transfer reactions. Solvation effects specific to Ru ammines, as well as direct involvement of the anion in the activation process, are indicated.

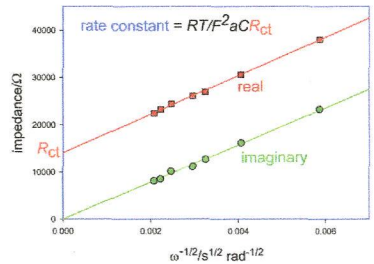

2769 S dx.doi.org/10.1021/ic400118p

Density Functional Theory Calculations of UO_2 Oxidation: Evolution of UO_{2+x}, U_4O_{9-y}, U_3O_7, and U_3O_8

D. A. Andersson,* G. Baldinozzi, L. Desgranges, D. R. Conradson, and S. D. Conradson

Formation of UO_{2+x} derived from the fluorite structure was investigated by density functional theory (DFT) calculations. We identify stable line compounds at the $U_4O_{8.889}$, U_3O_7, and $U_3O_{7.333}$ compositions. Although the transition from fluorite to the layered U_3O_8 structure occurs at U_3O_7 or $U_3O_{7.333}$, the fluorite-derived compounds are favored up to $UO_{2.5}$, that is, as long as the charge-compensation for adding oxygen atoms occurs via formation of U^{5+} ions, after which U_3O_{8-y} becomes more stable.

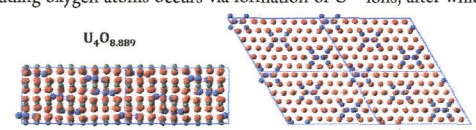

dx.doi.org/10.1021/ic400182u

Lanthanide-Porphyrin Hybrids: from Layered Structures to Metal–Organic Frameworks with Photophysical Properties

Jan Demel, Pavel Kubát, Franck Millange, Jérôme Marrot, Ivana Císařová, and Kamil Lang*

The control of reaction conditions allowed the synthesis of the rare-earth layered hydroxides with intercalated sulfonated porphyrins within the hydroxide layers or the incorporation of porphyrin units into the MOF possessing the features needed for effective photofunctional materials. The structure of the MOF was characterized in detail. The capability of the MOF to produce $O_2(^1\Delta_g)$ opens the possibility of designing novel multifunctional porphyrinic MOFs with tuned photoresponse and porosity.

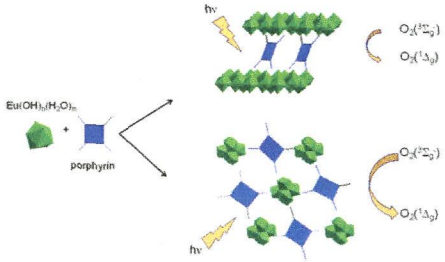

S Supporting Information available via online article